Contents lists available at ScienceDirect

Heliyon

Research article

Crystallographic investigation, Hirshfeld surface analysis, NLO characterization and experimental spectral (UV and NMR) studies with DFT probe on(R)-9-(2-hydroxy propyl)adenine

S. Sharmila Tagore [a], J. Swaminathan [b], D. Manikandan [c], S. Gomathi [c], N. Sabarinathan [d], M. Ramalingam [e], V. Sethuraman [c,*]

[a] Department of Chemistry, M.R. Govt. Arts College, Mannargudi, Tamilnadu, India
[b] Department of Chemistry, A.V.C. College of Engineering, Mayiladuthurai, Tamilnadu, India
[c] Department of Chemistry, Periyar Maniammai Institute of Science and Technology, Vallam, Thanjavur, Tamilnadu, India
[d] Department of Chemistry, Presidency College, Chennai, Tamilnadu, India
[e] Department of Chemistry, Bon Secours College for Women, Thanjavur, Tamilnadu, India

ARTICLE INFO

ABSTRACT

In this study, (R)-9-(2-hydroxy propyl)adenine (HPA) is the molecule of interest for investigation. The XRD from single crystal of HPA has been used to extract its structural features. Since HPA crystallised in a non-centro symmetric space group $P2_12_12_1$, its NLO property was studied and it was found to exhibit very good SHG activity. To explore the intermolecular interactions the generated Hirshfeld surface has been investigated along with 2D-fingerprint plots. The experimental electronic and NMR spectra taken in the UV-visible and radio frequency regions respectively for HPA have been corroborated in correlation with theoretical predictions at Density Function Theory using 6-311++g (d, p) basis set. The experimental XRD geometrical parameters, chemical shifts of ^{13}C and ^{1}H and λ_{max} values of HPA fit satisfactorily with the corresponding theoretically obtained numerical values as well as the stimulated spectrograms with the experimental ones. Further to explore the electronic structure, the MESP surface has been generated and investigated. The thermodynamic, kinetic and chemical reactivity features have been explored by means of frontier molecular orbitals of HPA.

1. Introduction

One of the important constituent aromatic bases of the nucleic acids DNA and RNA is the purine nucleobase adenine [1]. In RNA, adenine is attached to ribose sugar forming the nucleoside adenosine, whereas in DNA, it is bonded to deoxyribose sugar giving the nucleoside deoxyadenosine. Adenosine linked sequentially to three phosphoryl groups forming adenosine triphosphate has the key role in cellular metabolism involving chemical reactions of energy transformations. The biological activities, especially the antiviral and the restriction in the proliferation of cancer cells, are the criteria for the prevailing research interest on adenine and its derivatives [2]. The effect of a variety of new purine nucleosides and their derivatives on cancer [3, 4, 5, 6], viruses [7] and their potent hypoglycaemic activity [8] exhibit their importance in the field of structural biology.

In the cancer treatment by gene therapy [9, 10] acyclic nucleoside analogues are widely used. In antiviral chemotherapy the main focus is that the newly designed nucleoside analogues should only inhibit virus replication without any impediment on the normal cellular processes [11].

Reverse Transcriptase studies show that adenine moiety holding a side chain of two carbon atoms at 9th position has been proved to be inactive against HIV-1, for example 9-[(RS)-2-hydroxy propyl]adenine does not have antiviral activity at all [12], while moderate activity has been confirmed if 3-hydroxypropyl unit is present at 9th position. Recent investigation [13] established the fact that R configuration has shown more inhibitor activity. Moreover the role of 9-(2-hyrdroxypropyl)adenine (HPA) as a fake substrate in the case of Varicella zostervirus thymidine kinases andherpes simplex virus has been revealed through docking studies [14].

In the enzyme-inhibitor complex formation stereo selectivity is an important factor in the case of 9-substituted adenines having a chiral centre [15, 16, 17] and it is evident that the S-enantiomer of 9-(2, 3-dihydroxypropyl)adenine, has blocked the duplication of a number of DNA and RNA viruses, for example vesicular stomatitis, herpes simplex,

Table 1. Detailed Crystal data values of HPA.

Crystal Data	HPA
Formula	$C_8 H_{11} N_5 O$
CCDC number	1421496
Formula Wt.	193.22
Crystal System	Orthorhombic
Space group	$P2_12_12_1$ (No. 19)
a (Å)	4.6193 (1)
b (Å)	13.0277 (4)
c (Å)	15.3429 (5)
α, β, γ (°)	90, 90, 90
V (Å^3)	923.32 (5)
Z	4
D (calc) [g/cm^3]	1.390
μ(MoKα)[/mm]	0.099
F (000)	408
Crystal Size (mm)	0.30 × 0.30 × 0.35
Temperature (K)	293
Radiation (Å)	MoKα 0.71073
Theta Min-Max [Deg]	2.7, 25.0
Tot., Uniq. Data, R (int)	8639, 1631, 0.030
Observed data	1560
N_{ref}, N_{par}	1631, 140
R, wR2, S	0.0248, 0.0661, 1.09
min hkl	-5 -15 -18
max hkl	5 15 18
GooFS on F2	1.086

vaccinia and measles. Thus the compound 9-[(2-hydroxyethoxy) methyl] guanine (acycloguanosine) similar to the above one showed selective inhibitory activity to herpes viruses. The anti-herpes activity of acyclo-guanosine takes place *via* the phosphorylation of acycloguanosine to tri-phosphate in the herpes-attacked cells, which then blocks the herpes virus DNA polymerisation more than cellular DNA synthesis. The (R)-9-(l-hydroxy-2-alky1) adenine and (S)-9-(2-hydroxypropy1)adenine are found to have improved inhibitory action on adenosine deaminase over their respective enantiomers [18, 19, 20, 21].

To combat against HIV, adenosine monophosphate, 9-[2 (phospho-nomethoxy)ethyl] adenine and (R)-9-[2-(phosphonomethoxy)propyl] adenine bearing acyclic moiety have been shown to be effective and potential reagents [22, 23, 24] selectively. It has been reported [25] that the binding of ligands having adenine residues with enzyme occurs through hydrogen bond framework involving the donor residue near N1 and acceptor residues around 6-amino functional group.

In view of the above mentioned biological activities of adenine derivatives, we hope the spatial disposition of HPA atoms, particularly in the side chain, reported as in the case of 2-formylpyridine derivatives [26] would be of much help in the investigations of HPA's biological activities and for that reason, we did this investigation, by means of XRD and spectral analyses, supplemented with theoretical tools, DFT and Hirshfeld Surface through CrystalExplorer, as little work of these types of studies were found in the literature survey except the crystal structure of the Thymidine Kinase protein with racemic HPA [27].

2. Experimental details

The HPA obtained from Sigma-Aldrich, India has been dissolved in ethanol and THF (v/v 1:1) mixture and heated to 40 °C with constant stirring. After 30 min it was cooled to 25 °C. Colourless crystals were found to separate after a couple of weeks, from the mother liquor.

For the collection of X-ray data, the instrument used was Bruker Kappa APEX-II CCD diffractometer with monochromatic MoKα radiation having a wavelength of 0.71073A. For integrating the collected data and

correcting for Larentz as well as polarization effects Bruker SAINT [28] was then put into use. Multi-scan method by means of SADABS [28] was invoked for absorption correction. The structure solution by direct method had been obtained through SHELXS97 [29] software. The refinement process had been carried out using SHLEXL97 [29] with full matrix least squares on F^2. For heavy atom refinement, anisotropic factors had been used. For the hydrogen atoms, they were geometrically positioned on their carrier atoms and isotropic refinement was done. The relevant XRD data and hydrogen bond framework informations have been collected in Table 1 and Table 2. The crystallographic details have been provided in the supplementary files *HPA.fcf* containing the structure factor information (S1), *HPA.cif* containing crystallographic information (S2), HPA.checkcif.docx (S3) and HPA.sup.docx containing all the crystallographic tables with titles and other information (S4).

To get ^{1}H NMR and ^{13}C NMR spectra Avance 300 MHz instrument was used and the spectra were taken using (D6)-DMSO solvent. The electronic spectral data were collected in SHIMADZU UV-2550 instrument. For all the experimental X-ray and spectral data collection, the instruments available at SAIF, IITM, Chennai, Tamil Nadu, India were made use of. For the NLO measurements, the instrumental facility at B.S. Abdur Rahman Crescent University, Chennai, Tamilnadu, India was used.

3. Computational details

In this investigation, for all computations, the state-of-art B3LYP of Density Functional Theory (DFT), was followed [30] that had been implemented through Gaussian 03W/09W [31, 32] suit of programmes. The factors that DFT is computationally not demanding in spite of reliable predictions made us to choose this level of computations inspite of its inability to reproduce dispersive forces accurately [33]. To account suitably for orbital contraction in molecular environment, diffuse nature of non-bonding electrons and shifting the centre of orbitals in small rings, we had chosen the well-known 6-311++g (d, p) basis set, which is more adaptable in the valence region if hydrogen bond interaction is present. Initial geometrical structure constructed from the XRD co-ordinates was optimized invoking gradient geometry optimization with complete relaxation. The optimized geometry at stationary point had been characterised by inspecting the absence of imaginary frequencies. Nuclear magnetic shielding tensors of ^{1}H and ^{13}C-NMR have been computed by GIAO method at B3LYP/6-311++g (d, p), including solvent effect through PCM option. The gas phase as well as in the appropriate solvent (PCM model), vertical electronic excitation calculations have been done with time dependent-DFT. From the experimental and theoretical results, suitable inferences have been arrived at, after comparison with experimental results.

4. Results and discussion

4.1. Crystal structure analysis of 9-(2-hydroxy propyl) adenine (HPA)

The asymmetric unit of the crystal holds only one HPA molecule in orthorhombic space group $P2_12_12_1$. The dihedral angle between the adenine ring moiety and the side chain hydroxy propyl unit is determined to be 81.60 (8)°. The torsion angles -57.35 (15)° and -176.84 (12)° borne by N9-C11–C12-O14 and N9-C11–C12–C13 frameworks respectively and also -54.00 (16)° and 124.47 (13)° borne by C8–N9–C11–C12 and C4–N9–C11–C12 frameworks respectively are the key factors of the molecular conformation of HPA, with the 2-hydroxypropyl group (–CH2–CHOH–CH3) attached to N9 of imidazole unit of HPA. The following Figure 1 displays the ORTEP diagram of HPA.

The linking of N10 amino group to ring N3^{ii} atoms (Symmetry code: 2-x,-1/2 + y, 3/2-z) of adenine units of HPA with hydrogen bond interaction N–H…N results in intermolecular interaction among the neighbouring HPA molecules and this mode of connection with the said type of hydrogen bond interaction prevailing throughout is the basis for the formation of a supramolecular zig-zag chain in a plane. The N–H…O, O–H…N and C–H…N hydrogen bond frameworks occurring between
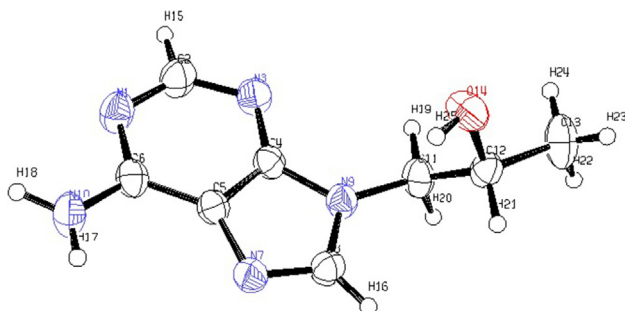
Table 2. Hydrogen bond-metrics for HPA.

D–H....A	[ARU]	D–H	H...A	D...A	D–H...A
		(Å)	(Å)	(Å)	(o)
N (10)–H (17)…O (14)	[3456.01]	0.851 (14)	2.341 (14)	3.1366 (16)	155.8 (13)
N (10)–H (18)…N (3)	[4655.01]	0.910 (15)	2.188 (15)	3.0790 (17)	166.2 (14)
O (14)–H (25)…N (7)	[3556.01]	0.89 (2)	1.93 (2)	2.7676 (15)	156 (2)
C (8)–H (16)…N (7)	[3456.01]	0.93	2.55	3.3686 (18)	148
Translation of ARU-code to Equivalent Position Code					
i) [3556] = 1/2 + x, 1/2-y, 1-z					
ii) [4655] = 1-x, 1/2 + y, 1/2-z					
iii) [3456] = -1/2 + x, 1/2-y, 1-z					

Figure 1. The ORTEP diagram of HPA (50% probability thermal displacement ellipsoids).

adjacent supramolecular chains generate two ring motifs, viz., R_2^2 (7) and R_2^2 (10) as in Figure 2. The N–H…O and O–H…N connect amino N10 and ring N7 atoms and hydroxy O14^{iii} (symmetry code: -1/2 + x, 1/2-y, 1-z) atom of symmetry related HPA molecule in adjacent plane. The C–H…N hydrogen bond framework bridges adenine C8–H group and ring N7^{iii} (symmetry code: -1/2 + x, 1/2-y, 1-z) atoms and hydroxy O14 group with ring N7^{i} (symmetry code: 1/2 + x,1/2-y, 1-z) atom of HPA. The above mentioned two ring motifs in turn generate R_6^6 (31) motif, linking six symmetry related HPA molecules together. The presence of such weak and strong hydrogen bond interactions produce a two dimensional supramolecular zig-zag sheet, propagating along *b* axis as shown in Figure 3.

Further the aromatic off set π-π stacking interactions between five (Cg1) and six membered (Cg2^{iv}) (Symmetry code: (iv) -1+x, y, z) ring

cloud of adenine units of symmetry related HPA molecules lead to the stabilization of zig-zag sheets (Figure 4), with the corresponding centroid to centroid and perpendicular distances being 3.6057 (8) Å, 3.298 Å and the slip angle is measured to be 24.64°.

Based on the hydrogen bond distances, O14–H25 … N7, N10–H18 … N3 and N10–H17 …O14 may be considered as strong hydrogen bonds since H … A distance is less than 2.4 Å in addition to the fact that the hydrogen bond frame work is formed by two strongly electronegative atoms. The hydrogen bond C8 – H16 … N7 may be considered as weak as the H … A distance falls beyond 2.4 Å and involves only one electronegative atom [34]. In the short and medium range hydrogen bonds, the electrostatic interactions play a dominant role which varies inversely with H …A distance.

4.2. Hirshfeld surface analysis of HPA

In general organic crystals are the resultants of intermolecular interactions/contacts among the constituent molecular species and so to have a clear insight into the various factors contributing to the crystalline HPA, a Hirshfeld surface (HFS) of isovalue = 0.5, for the chosen promolecule (P) obtained from crystallographic *cif* file of HPA, has been generated by means of CrystalExplorer 17.5 [35], based on the reported Eq. (1) [36].

$$w_A(r) = \sum_{i \in molecule\ A} \rho_i^{at}(r) \Bigg/ \sum_{i \in crystal} \rho_i^{at}(r) \tag{1}$$
$$= \rho_{promolecule}(r)/\rho_{procrystal}(r)$$

The Hirshfeld isosurface carved by the isovalue of $w_A(r) = 0.5$, mapped over the d_{norm} function of HPA (-0.610to +1.290 arbitrary units)
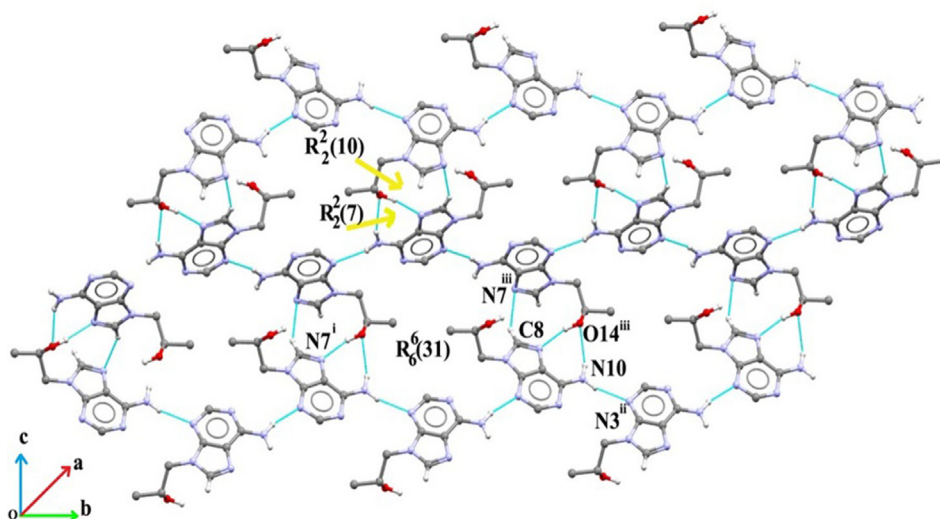
Figure 2. Hydrogen bonds supramolecular assembly N–H…N, O–H…N, N–H…O and C–H…N. [Symmetry codes: (i) 1/2 + x,1/2-y, 1-z; (ii) 2-x,-1/2 + y, 3/2-z; (iii) -1/2 + x,1/2-y, 1-z].
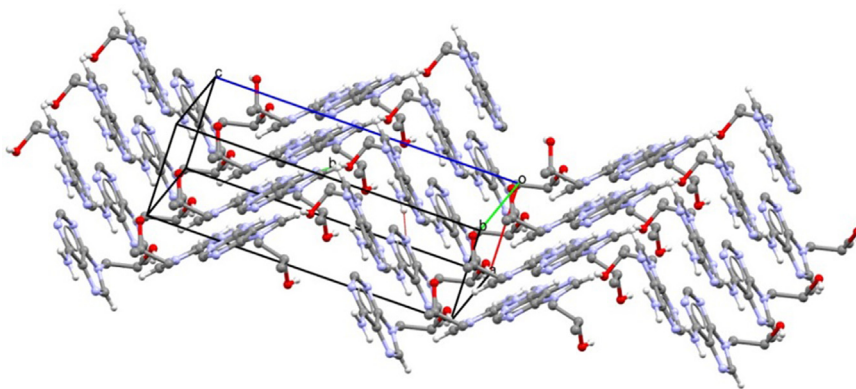
Figure 3. Supramolecular zig-zag sheet appearance in 2-D view.

from the CIF file, is shown below: d_{norm} is the sum of $d_i + d_e$ where d_i and d_e are the normalised extensions from a chosen point on the HFS to the inside and outside atoms correspondingly (Figure 5). The various colour codes on the HFS indicate the type of interatomic contacts/interactions, such as red, blue and white colours correspond to shorter, equal and longer than summation of van der Waals radii of atom-pair in contact [37]. For better visual effect of the promolecule within the HFS, surface transparency is enabled. The d_e surface Figure 5 (a) indicates hydrogen bond acceptor regions conspicuously, while the d_{norm} surface Figure 5 (b) exhibits both the acceptor and donor regions as red spots, of course with varied intensities. Figure 5 (c) and (d) represent the promolecule P being surrounded by exterior molecules E1 to E6.

The atoms within 3.8 Å of the Hirshfeld's surface with all possible intermolecular hydrogen bond interaction of types N–H...O, N–H...N, O–H...N, C–H...O and C–H...N, etc., are also displayed and the intensity of the red patches are proportional to the strength of the interaction

energy, varying with H-bond distance and angle of H-bond framework. The HPA promolecule within the HFS has some five potential sites for intermolecular hydrogen bond interaction with the nearby surrounding HPA molecules at the exterior of HFS, of which N3, N1, N7 and O14 are acting as hydrogen acceptors with lone pair electrons, while N10 is capable of donating H17 and H18 to O14 and N3 to the nearby HPA molecules at the exterior of HFS in the crystal respectively. The various hydrogen bond frame works with atom-pair distances and angles are tabulated in Table 3.

4.2.1. 2D fingerprint plot

With a view to quantifying and delineating the type and nature of intermolecular interactions/contacts, between the molecules inside and outside of the HFS, a 2D plot has been generated in terms of (d_e, d_i) pairs within 0.01Å, in which the fraction of points on HFS is a functional of d_e, and d_i and thus enables to identify the type of interactions. The colour code
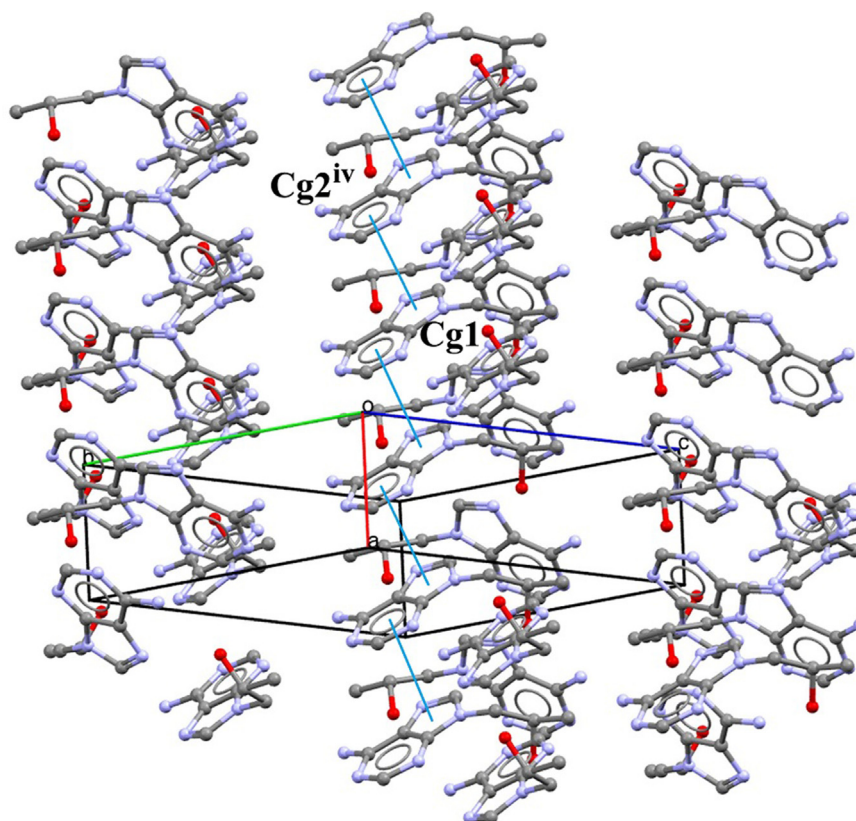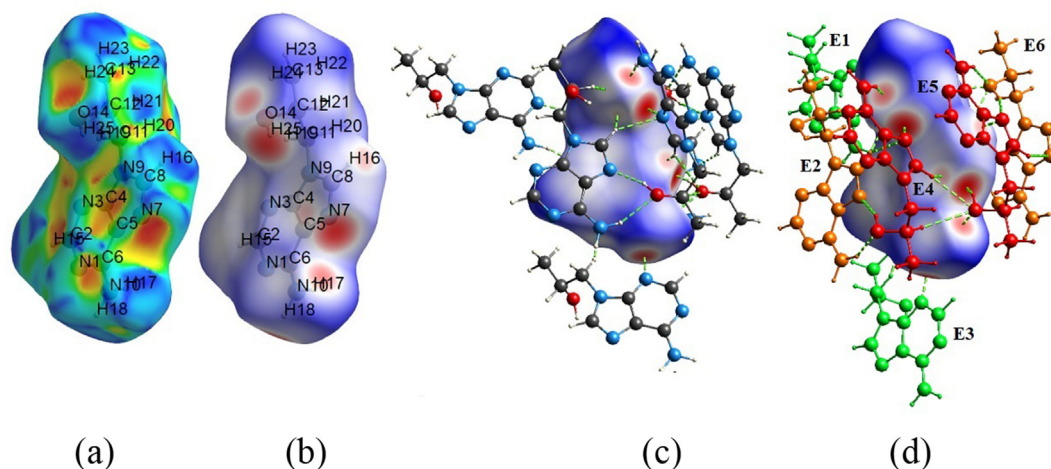

Figure 4. Stacking interaction binding adjacent sheets together. [Symmetry code: (iv) -1+x,y,z].

Figure 5. HFS (a) mapped with d_e; (b) mapped with d_{norm}; (c) and (d) promolecule P exteriorly surrounded by E1 to E6 molecules with hydrogen bond interactions in green dotted lines.

of the bin containing the (d_e, d_i) pairs is from blue through green to red. The blue coloured area with dots of varied intensities represent all the possible interactions across the HFS, both externally (d_e) and internally (d_i). The full fingerprint region ($d_i = d_e = 0$ to 2.4 Å) comprising all the strong/weak interactions/contacts appears with nearly diagonal symmetry comprising long spike type projections including smaller ones in between, at left downside (Figure 6 (a-e)). The various possible combinations of atom-pair interactions and the individual contributions to the overall interaction are shown in the interaction-matrix Table 4. The major contributor to the crystal packing is the short interatomic H…H interactions (46.9%) with intense scattering as evident clearly from Figure 6 (b). Interestingly the symmetric or asymmetric distribution of bins of X…Y/Y…X interactions, over the HS can be found by inspecting the off-diagonal elements (X…X) in Table 4. The entire interactions are covered fully in Figure 6 (a), while the remaining 2D plots Figure6 (b-e) correspond to H…H, H…N, H…C and H…O interactions with deviation from symmetric types because of difference in the quantum of interactions among the particular atom-pair, inside and outside the reference point on the HFS, involving slightly different environments within the crystal.

4.2.2. Interaction energy and energy framework

In the crystal system, the interaction energy is related to pair-wise intermolecular interaction using unperturbed electron densities and related properties as shown by Eq. (2) [39].

$$E_{tot} = E_{ele} + E_{pol} + E_{dis} + E_{rep} = k_{ele}E'_{ele} + k_{pol}E'_{pol} + k_{dis}E'_{dis} + k_{rep}E'_{rep} \quad (2)$$

For the interaction energy estimate we used the default CE-B3LYP

method, implemented in CrystalExplorer 17.5. We first created a cluster of 15HPA by choosing all nearby molecules within 3.8 Å around the promolecule at the centre. On analysing the various interacting pairs, we found that the molecules exterior to the promolecule were in linear parallel and orthogonal alignments. The various interaction energies of promolecule with the specific nearby one with breakup details into electrostatic, polarisation, dispersion and exchange repulsion, seem to be the critical controlling factors in crystal packing and are shown in the following Table 5.

The interaction energies above |15| kJ/mol alone are considered and the same are exhibited in Figure 7, with dotted lines of interacting molecules centroids.

The total interaction energy in between the centroids (around N5 of imidazole unit) of promolecule and E1, E2 and E3 are -67.4 kJ/mol, -40.7 kJ/mol and -30.2 kJ/mol respectively and these values correlate very well with the corresponding hydrogen bond framework. Moreover the total interaction energy displayed is not exclusively the quantified hydrogen bond energy, but it has the major share from the electrostatic and dispersion energy components of E_{tot} (interaction energy), the vital parts in crystal packing.

The following Figure 8 (a) is the representation of Hirshfeld surface mapped over the shape index from -0.989 to 0.996, having the visible blue coloured convex and red coloured concave regions correlated to hydrogen-bond donating and hydrogen–bond accepting moieties respectively, along with the encircled regions involving the π…π contacts revealed by closely spaced blue and red coloured tips of the triangles. Figure 8 (b) shows the weak π….π stacking with flat HFS, encircled by red ellipse.

Table 3. Atom-pair distances and angles of H-bond framework from HFS analysis.

S.No.	H-bond framework	H-bond length* (Å)	Angle (°) of H-bond framework
1	N7…H25–O14	1.846	154.8
2	N3…H18–N10	2.092	165.5
3	N10–H18…N3	2.092	165.5
4	N10–H17…O14	2.198	154.1
5	C12–O14…H17	2.198	139.0
6	N7…H16–C8	2.418	145.7
7	C12–O14…H16	2.516	145.3
8	N1…H19–C11	2.567	152.2
9	C12–O14…H21	2.603	154.1

* Van der Waals radii summation of H (1.17) and O (1.40)→2.57 Å & H (1.17) and N (1.50)→2.67 Å [38].
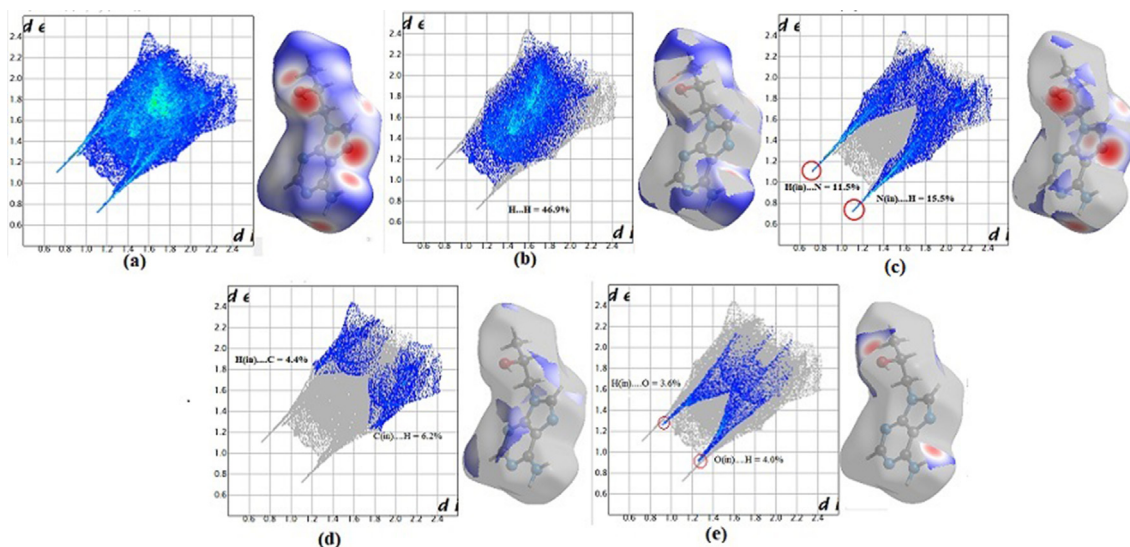
Figure 6. (a) The full 2D fingerprint plot of HPA with delineation into individual. interactions (b) H…H, (c) N…H (d) C…H and (e) O…H.

Table 4. Percentage Breakup details of 2D fingerprint area of interactions into individual type – for close contacts between atoms inside and outside the HFS.

HF in \ HF out	C	H	N	O	Tot
C	**1.3**	6.2	2.5	0	10
H	4.4	**46.9**	11.5	3.6	66.4
N	2.2	15.5	2.0	0	19.7
O	0	4.0	0	0	4
	7.9	72.6	16	3.6	100.1

4.3. NLO study

Kurtz-Perry powder method [40] was used to study the second harmonic generation of the HPA crystal using the instrument QUANTA RAY Model LAB – 170–10. When the powdered sample of the crystal was illuminated with Q switched Nd: YAG LASER emitting a wavelength of 1064 nm, the frequency doubling was observed by the emission of green light of wavelength 532nm. The compound being organic, urea was used as the reference material. The output energy for the sample was found to be 11.8 mJ compared to the reference value of 9.56mJ. Hence the SHG efficiency of the material is found to be 1.23 times greater than urea. Despite the fact that the dipole moment of urea (3.9 D) is higher than that of HPA (3.1 D), the higher polarizability (136.64a.u.) of the latter over the former (34.06 a.u.) supports the HPA's SHG of 2.02 times of urea, based on the hyperplarizability (β) estimates (β of urea = 93.75 a.u. and HPA = 189.65a.u.). Notwithstanding the fact that NLO response is ~2 times that of the reference

urea in the theoretical estimate, the value of 1.23 times over urea in the experimental evaluation, shows that HPA may be a good candidate in NLO applications/optoelectronics.

4.4. Computational studies

4.4.1. HPA molecular structure analysis

Figure 9 exhibits the sequence of atom numbering adopted for HPA in all theoretical computations in this study. Table 6 contains the selected geometrical parameters of HPA obtained by theoretical and experimental methods.

For neutral HPA, majority of theoretical and XRD structural parameters were found to be in good coincidence with one another. The Pearson's positive correlation coefficients 0.9945, 0.9869, 0.92153 and 0.97232 in respect of bond lengths, bond angles, dihedral angles and all the parameters put together respectively also support almost the one-to-one correspondence between calculated and experimental geometrical parameters. The reason for the variation of the calculated values from those of experimental values is due to the neglect of the crystalline state intermolecular forces. This results in the release of crystal packing force causing the large deviation in dihedral angles.

The overlayed structures (green-experiment; red-calculated) are shown in Figure 10 to illustrate the good agreement between theory and experiment. The variations between selected pairs are shown for comparison.

#### 4.4.2. ^{1}HNMR and ^{13}CNMR spectral investigations

4.4.2.1. Aromatic hydrogen atoms. Figure 11 and Figure 12 show the theoretical ^{1}H and ^{13}C NMR spectra of HPA while Figure 13 and Figure 14 show their corresponding experimental spectra. A comparion of the currently recorded spectra and the already reported spectra [41] shows that the agreement between the two is good. Table 7 displays the current experimental and theoretically calculated chemical shift values. The Pearson's positive correlation coefficients 0.8683 and 0.9993 in respect of ^{1}HNMR and ^{13}CNMR respectively also support the almost the one-to-one correspondence between calculated and experimental NMR values of HPA.

In accordance with theory H15 and H16 proton signals of aromatic heterocyclic ring have been calculated to be 8.461 and 7.974 δ respectively, satisfactorily coinciding with the observed values of 8.13 and 8.04

Table 5. Interaction Energies (kJ/mol)of the promolecule with the surrounding molecules within 3.8 Å from HFS(R - distance between molecular centroids in Å).

N	Symop	R	E_{ele}	E_{pol}	E_{dis}	E_{rep}	E_{tot}
2	x+1/2, -y+1/2, -z	5.09	-77.1	-17.5	-33.6	91.3	-67.4
1	x, y, z	4.62	-6.2	-4.5	-41.7	26.0	-30.2
0	x, y, z	13.03	0.7	-0.1	-0.4	0.0	0.3
1	-x+1/2, -y, z+1/2	10.11	0.4	-0.1	-1.5	0.1	-0.9
0	-x+1/2, -y, z+1/2	8.91	-2.1	-0.3	-6.0	2.3	-6.3
0	-x, y+1/2, -z+1/2	7.84	-38.8	-9.3	-19.1	38.5	-40.7
1	-x+1/2, -y, z+1/2	12.41	-0.3	-0.0	-0.2	0.0	-0.5
0	-x+1/2, -y, z+1/2	11.46	-0.1	-0.0	-0.4	0.0	-0.5
0	-x, y+1/2, -z+1/2	13.66	-0.2	-0.0	-0.1	0.0	-0.3
0	x, y, z	13.82	0.7	-0.0	-0.2	0.0	0.5
0	-x, y+1/2, -z+1/2	10.28	0.4	-0.1	-0.8	0.0	-0.3
1	x+1/2, -y+1/2, -z	8.28	-0.1	-0.1	-1.4	0.0	-1.4
0	-x, y+1/2, -z+1/2	15.19	-0.2	-0.0	-0.0	0.0	-0.3
0	-x, y+1/2, -z+1/2	7.74	-6.4	-1.3	-12.9	5.7	-15.4

Scale factors for B3LYP/6-31G (d,p): 1.057(k_{ele}), 0.740 (k_{pol}),0.871 (k_{dis}) and 0.618 (k_{rep}).
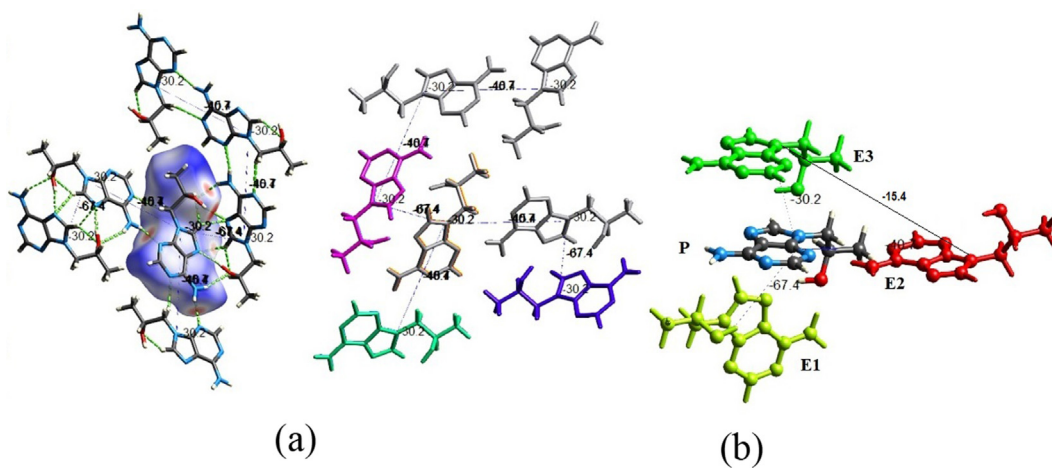
Figure 7. Interaction energy between the promolecule with outside HFS within 3.8Å. (a) with and without HFS, (b) promolecule's interaction with selected molecules outside HFS.
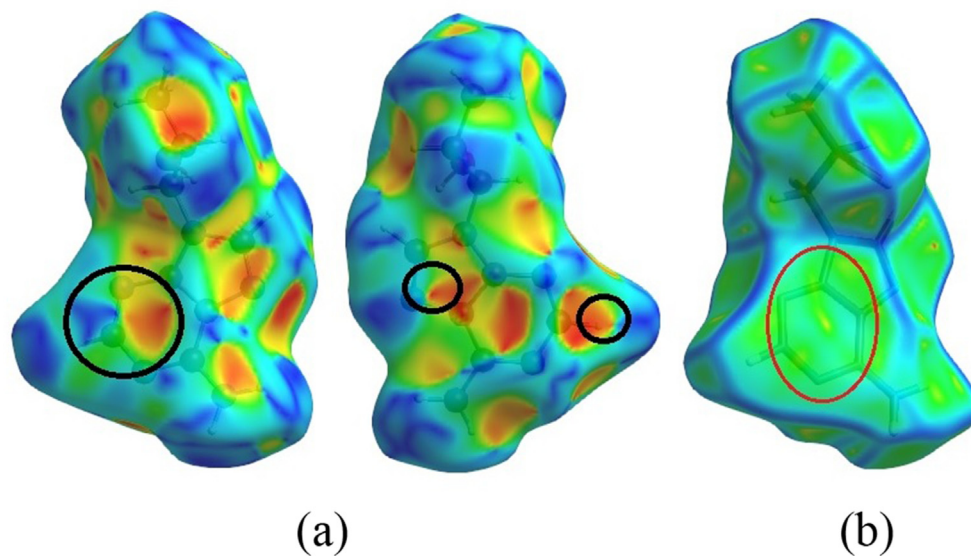
Figure 8. Hirshfeld surface mapping over (a) shape index (-0.989 to 0.996) and (b) curvedness (-3.544 to 0.256).
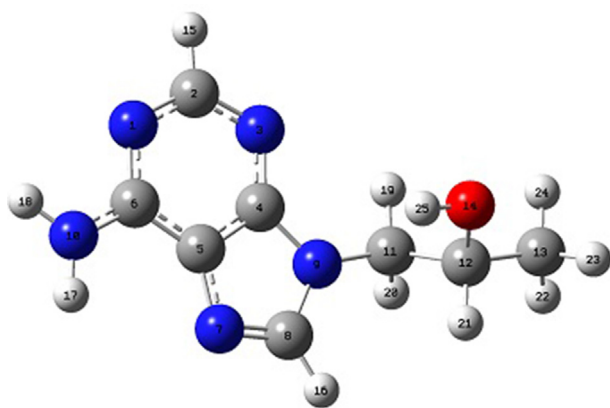
Figure 9. Atom numbering of HPA followed in computations.

δ with errors of chemical shift values from the theoretical prediction being for H15 ~4%, while for H16 only ~1%.

The dihedral angles H17–N10–C6–N1 and H18–N10–C6–C5 measured as 177.0° and 175.2° respectively show the near planarity of the –NH₂ group with the heterocyclic ring attached. In general the resulting amino protons chemical shift values are in the range 3–8 δ in experimental observations. This may be due to bonding of these protons with electronegative N atom as well as exchange reactions with solvent D₂O. A close analysis of the experimental spectrum reveals that the two proton singlet signal occurring at 7.18 δ is due to the amino protons H17 and H18. The occurrence of one signal is due their identical nature and also due to their fast exchange reactions with D₂O solvent. . But in calculation these two amino protons are found to have two different chemical shift values namely 5.48 and 5.071 δ. The reason is the spatial orientations of these two H atoms are associated with different chemical environments during single molecule computation without rotation about C6–N10 bond, unlike the real situation in the experiment.

4.4.2.2. Side chain hydrogen atoms. As expected, the methylenic protons H19 and H20 of the acyclic side chain attached to N9 of imidazole ring system exhibited a multiplet resonance signal with chemical shift values in the range of 3.96–4.12δ, when measured in the instrument. The split pattern signals of H19 and H20 of multiplets are explained by considering the attachment of this unit (–CH₂–) to the adjacent asymmetric carbon holding –H, –OH and –CH₃ groups, which makes this –CH₂- dissymmetric/diastereotopic, with each proton giving a doublet due to ²J coupling, these in turn coupling with H21 (³J).The theoretically obtained chemical shift values around 3.784 δ and 4.438 δ identified with H19 and H20 respectively, with a difference in chemical shift value of ~0.7 δ, may be ascribed to the different spatial disposition of the hydrogen atoms, experiencing diverse magnetic environment during the computational process.

The chemical shift value 4.158 δ calculated quantum chemically is assigned to asymmetric H21, which very much matches with the one proton multiplet observed experimentally between 3.96 and 4.12 δ. Normally alcoholic resonance signal would appear in the range of 0.5–5 δ involving chemical exchange and hence the experimental chemical shift of 5.03 δ has been associated with H25 of the hydroxyl group. But the DFT estimate at a very low chemical shift of 1.156 δ contrary to the experimental one at a much higher value may be attributed to frozen status of H25 in the calculation.

As anticipated, the three methyl protons (H22, H23 and H24 attached to C13) gave a doublet at 1.06 δ due to scalar coupling with H21 on adjacent C12, revealing the identical chemical and magnetic environment because of the rotational frequency of the methyl protons around C13–C12 bond. The neglect of aforementioned chemical equivalence of methyl protons and the frozen nature of rotational frequency of the methyl moiety in DFT calculation, lead to three different resonance signals at 1.387, 1.383 and 1.233 δ.

4.4.2.3. Aromatic carbon atoms. Generally the aromatic carbon atoms are expected to have chemical shift values in the range of 122.2 δ and the heterocyclic aromatic carbon atoms higher than this value. Each of carbon atoms C2, C4, C6 and C8 having electronegative nitrogen atoms flanked on both sides are also experimentally found to have higher chemical shift values higher than 122.2 δ in the order, C6 > C2 > C4 > C8. The same order is confirmed through calculated values, in spite of their higher magnitudes. The C5, in the aromatic heterocyclic six membered ring, surrounded trigonally by N7, C4 and C6, without nitrogen atoms on either side has the resonance absorption at a lower value of 118.5 δ and is consistent with the relatively lower value of 125.367 δ theoretically calculated.

4.4.2.4. Side chain carbon atoms. On the basis of electronegativity of atoms bonded to carbon atoms, the carbon atoms of the aliphatic side chain at N9 of HPA should be in the order, C12 > C11 > C13, and the calculated chemical shift values of 73.98, 53.589 and 23.409 δ are in conformity to that prediction. The corresponding experimental values of 64.6 δ, 50.1 δ and 20.8 δ even though less than the calculated values confirm that the trend is exactly the same, revealing the good coincidence between theory and experiment.

4.4.3. UV spectral analysis of HPA

The experimentally observed and calculated vertical energies of the electronic excitations and the corresponding λ_max in aqueous medium have been collected in Table 8. Figure 15 and Figure 16 show the experimentally recorded and theoretically simulated UV spectra.

The computed excitation at 4.8958 eV composed of antepenultimate HOMO (49)→ LUMO+1 (53), HOMO(51)→LUMO(52) and HOMO(51)→ LUMO+1 (53), with the probability of that excitation f = 0.2797, does not show any single dominant component. For this excitation the corresponding Natural Transition Orbitals (NTOs) have been generated, to realise the NTO transition that occurs from excited particle (occupied) to the empty hole (unoccupied) [42]. The component transitions of this excited state are three and the corresponding NTOs computed for this state result in two pairs. The experimentally observed absorption at 262 nm agrees satisfactorily with the calculated value of 253.25 nm and the deviation is only ~3.3%.The theoretically calculated λ_max value of 210.04 nm at 5.9029 eV excitation very well correlates with the observed value of 206.50 nm and the deviation is around 2%. The calculated excitation at 5.999 eV composed of HOMO(51)→ LUMO+4 (56), and HOMO(51)→ LUMO+5 (57), with the probability of that excitation f = 0.0006, is not associated with any single dominant component and hence the corresponding NTOs have been produced, to recognise the NTO transition from excited particle (occupied) to the empty hole (unoccupied) [43]. The component transitions of this excited state are two and the corresponding NTOs computed for this state result in two pairs. Notwithstanding the fact that f = 0.0006, the calculated excitation line at 206.68 nm exactly coincides with the experimental value of 206.50 nm. Spatial forms of important MOs participating in UV-Vis spectrum are plotted in Figure 17. The figure shows, that localization or delocalization of electrons vary in occupied and unoccupied MOs.

4.4.4. Molecular electrostatic potential (MESP)Analysis

Around a molecule, points of same local electron density probability generated from the appropriate eigenfunctions on joining would describe a 3D surface, called electron density isosurface, such that its volume is directly related to percentage of total electron density enclosed [44]. Then the molecular electrostatic potentials are calculated with reference to a unit positive charge at points $\rho(r')$ around the electron density isosurface, in terms of its interaction with the electric field produced by the nuclei and electrons of the molecule, which is unperturbed by the test unit positive charge. These MESPs are mapped over the electron density isosurface with colour codes, based on the sign and quantum of

Table 6. Structural parameters of HPA.

Parameters	Calculated	Experimental
Bond length(Å)		
C11–C12	1.528	1.5147 (19)
C12–C13	1.527	1.5102 (19)
C12–O14	1.434	1.4153 (17)
C2–N3	1.334	1.3289 (17)
C4–C5	1.396	1.3834 (18)
C5–C6	1.408	1.4060 (18)
C5–N7	1.382	1.3838 (17)
C6–N1	1.343	1.3476 (18)
C6–N10	1.354	1.3395 (18)
C8–N9	1.382	1.3598 (16)
N1–C2	1.341	1.3341 (18)
N3–C4	1.338	1.3457 (18)
N7–C8	1.310	1.3108 (17)
N9–C11	1.456	1.4649 (16)
N9–C4	1.379	1.3713 (16)
O14–H25	0.962	0.89 (2)
Bond Angle (°)		
C11–C12–C13	111.05	109.58 (11)
C11–C12–O14	111.53	111.36 (11)
C12–O14–H25	109.3	108.3 (15)
C13–C12–O14	107.06	108.06 (13)
C2–N1–C6	118.6	117.88 (10)
C2–N3–C4	111.6	110.52 (11)
C4–C5–C6	116.0	117.23 (12)
C4–C5–N7	111.0	110.56 (11)
C4–N9–C11	125.7	128.16 (10)
C5–C6–N1	118.8	117.95 (12)
C5–N7–C8	104.48	103.68 (11)
C8–N9–C11	127.75	125.94 (10)
C8–N9–C4	105.64	105.89 (10)
H17–N10–H18	120.3	117.4 (14)
N1–C2–N3	128.4	130.15 (13)
N3–C4–C5	126.6	126.21 (12)
N7–C8–N9	113.8	114.13 (12)
N9–C11–C12	113.3	112.17 (10)
N9–C4–C5	105.2	105.74 (11)
Dihedral Angle (°)		
C11–C12–O14–H25	-168.0	-156.10 (10)
C13–C12–O14–H25	70.6	76.12 (11)
C2–N3–C4–C5	0.1	-0.3 (2)
C4–C5–C6–N1	-0.3	2.78 (19)
C4–C5–N7–C8	0	-0.02 (16)
C4–N9–C11–C12	99.2	124.47 (13)
C5–C6–N1–C2	0.3	-2.45 (19)
C5–N7–C8–N9	-0.3	0.54 (15)
C8–N9–C11–C12	-79.0	-54.00 (16)
C8–N9–C4–C5	-0.4	0.79 (13)
N1–C2–N3–C4	0	0.8 (2)
N3–C4–C5–C6	0.1	-1.4 (2)
N7–C8–N9–C4	0.4	-0.87 (15)
N9–C11–C12–C13	-171.9	-176.84 (13)
N9–C11–C12–O14	66.5	-57.35 (14)
N9–C4–C5–C6	-179.7	178.54 (11)

interaction. The MESP (V_{MESP}) is calculated from the electronic wave functions shown by Eq. (3):

$$V_{MESP} = \sum_A \frac{Z_A}{|R_A - r|} - \int \frac{\rho(r')dr'}{|r' - r|} \tag{3}$$

Z_A-nuclear charge of atom A; R_A and r-the coordinates of A and the unit positive charge, and $\rho(r')$ - electron density at the chosen point r'. Suitable electron density integration provides V_{MESP}. The repulsion or attraction is explicitly correlated with V_{MESP} in the range $0 > V_{MESP} > 0$ that would assist to classify the substrate's type of reaction, i.e., electrophilic/nucleophilic/radical as well as non-covalent intramolecular. Importantly MESP mapping helps a lot not only to investigate the molecular structure but also the physiochemical property relationships [45, 46, 47].

The MESP of HPA, mapped over the isodensity surface with $\rho(r') =$ 0.0004 a.u. between -5.838e-2 (red) and +5.838e-2 (blue) at three different orientations are shown in Figure 18.

Figure 18 in reality provides an idea about the shape and size of the molecule as the surface is transparent for visualization, in addition to regions of negative potential (deep red), and positive potential (deep blue) with graded colouring such as light blue, yellow, green etc., from -0.05838a.u. to 0.05838a.u., as shown in the horizontal bar above the MESP diagram. Additionally the size, shape and ESP values of the molecule are indicated. The colour codes have the trend, red < orange < yellow < green < blue. The rich electron density in the region of the nitrogen atom is marked by red colour and it supports its electronegativity nature. The blue and red coloured areas in the projected surfaces of Figure 18 distinctly show nucleophilic and electrophilic regions respectively. The MESP of HPA clearly indicates the electron rich centres around nitrogen atoms N1, N7 and N9. Also, the MESP map confirms that the positive potential sites are around the hydroxyl hydrogen H25 indicated by blue colour followed by the region around amino hydrogens H17 and H18.

4.4.5. Frontier molecular orbital studies

The molecular eigenfunctions (LCAO-MO) with maximised (highest) eigenvalue holding a pair of/single electron(s) in a molecule in accordance with Pauli's anti-symmetrized principle and the immediate empty virtual one, well known as HOMO and LUMO respectively are generally the important molecular orbitals (MOs), otherwise known as Frontier Molecular Orbitals (FMOs) because of their significant role in chemical reactivity, stability, charge transfer processes, photo-excitation, magnetism and molecular electronics [48]. Despite the fact that DFT functional may not evaluate orbital eigenvalues precisely, Kohn Sham (KS) orbitals of density functional theory provide a theoretical and practical base for a better qualitative understanding of molecular orbitals [49, 50, 51]. The eigenvalues of the FMOs and the difference among them are very
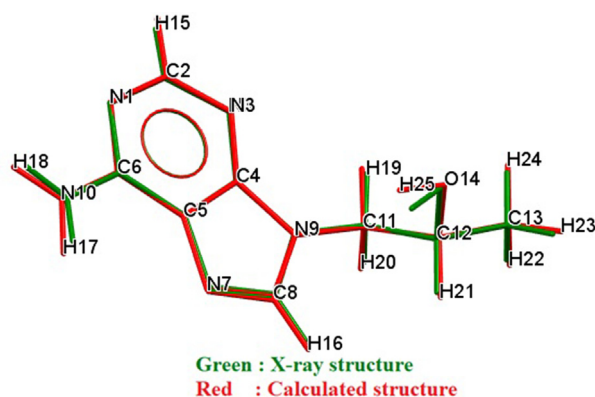
Figure 10. Overlay of crystal structure and DFT calculated structure; RMSD 0.0665Å.

H25…H25 → 0.418
H21…H21 → 0.108
O14…O14 → 0.107
H19…H19 → 0.132
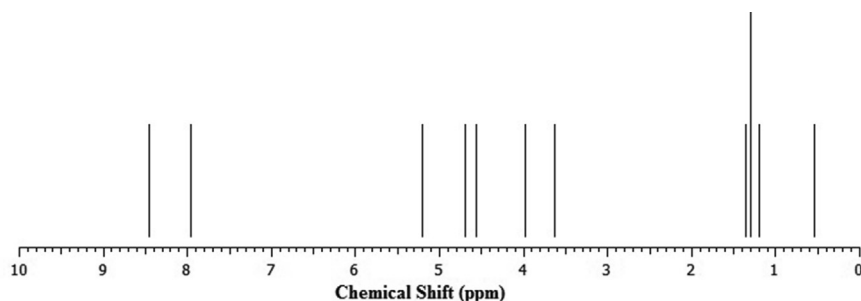H22…H22 → 0.177
H23…H23 → 0.167
H24…H24 → 0.208
N10…N10 → 0.127

Figure 11. Theoretical ^{1}HNMR spectrum of HPA.

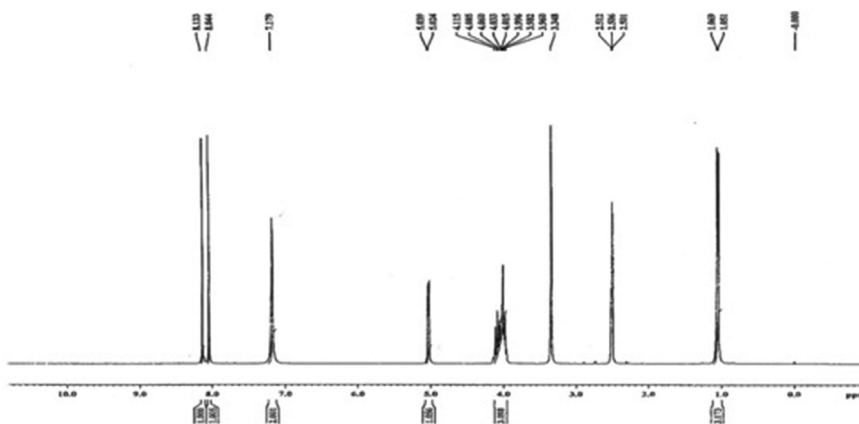**Figure 12.** Theoretical ^{13}CNMR spectrum of HPA.

important parameters in quantum chemical investigations of chemical reactivities. Normally small HLEG is associated with high degree of conjugation in the molecule, the reason being an appreciable amount of intra-molecular charge transfer from the electron releasing to the electron accepting groups through π-conjugation [52]. The chemical stability is directly proportional to the HLEG value [53, 54] and this fact has been recently exploited to analyse the bioactivity in terms of intra-molecular charge transfer [55, 56,].

The positive and negative parts of eigenfunctions 51 (HOMO) and 52 (LUMO) and the respective combined functions graphical representations with isovalue = 0.02 are shown in Figure 19. Inspection of HOMO and LUMO surfaces indicate that AOs from the heavy atoms of adenine skeleton contribute in the construct of π – type HOMO and π* - LUMO. As the energy gap (HLEG = 5.322eV) between these two FMOs is of

considerable magnitude, HPA seems to be thermodynamically a stable species with subdued chemical activity.

The chemical reaction of a substrate HPA with an electrophile or a nucleophile is largely controlled by the HMO-LUMO energies of the participating species in addition to their symmetry, i.e., an electrophilic reaction is favoured if the reagent's LUMO lies nearer to the high HOMO of the substrate while latter's LUMO proximity to the reagent's HOMO enhances nucleophilic reaction, provided thermodynamic stability of the substrate is not favoured. These predictions could be explained by means of global chemical reactivity descriptors evaluated from HOMO-LUMO eigenvalues.

For molecules with closed-shell electronic structure, the negative of RHF theory eigenvalue of HOMO according to Koopmans' theorem [48] could be identified with the first ionisation potential (IP). In accordance
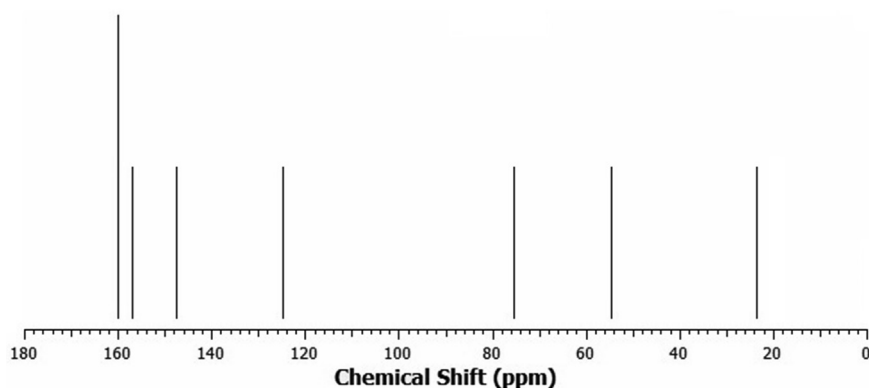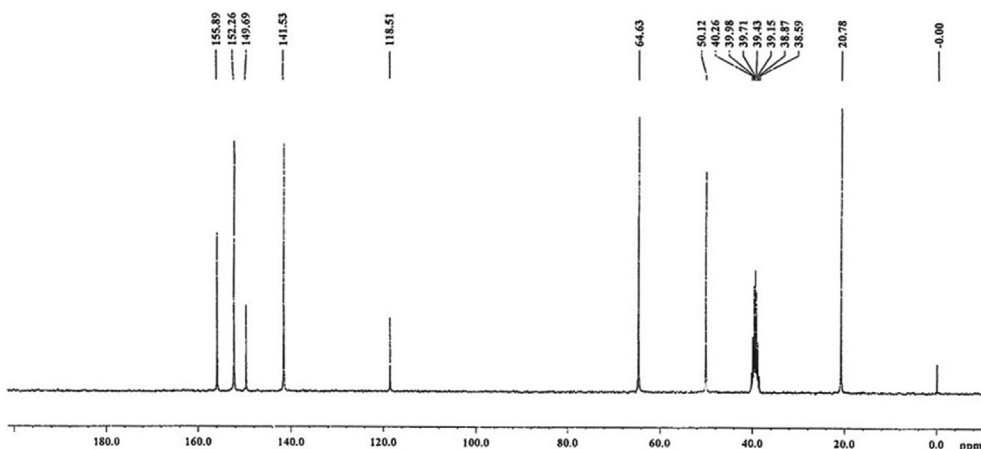

Figure 13. Experimental ^{1}HNMR spectrum of HPA.

Figure 14. Experimental ^{13}CNMR spectrum of HPA.

with Koopmans' theorem, the vertical ionisation potential and electron affinity values are given by the negative eigenvalues of Kohn-Sham's FMOs HOMO and LUMO respectively. As the energies of the HOMO, LUMO and gap between these two govern not only the typical chemical reactions of specific types but also the thermodynamic and chemical kinetic features of the system under analysis and hence the various global chemical reactivity descriptors such as chemical potential μ, hardness η, softness S, electrophilicity ω, electrodonating power $ω^-$, electroaccepting power and net electrophilicity $ω^±$ involving them have been evaluated [57, 58] and we hope it would help to analyse HPA's interaction in

biological systems. The global chemical reactivity descriptors, calculated as per the formulae given below (4) are collected in Table 9.

Chemical Potential $\mu = \dfrac{\varepsilon_{HOMO} + \varepsilon_{LUMO}}{2}$

Global Hardness $\eta = \varepsilon_{LUMO} - \varepsilon_{HOMO}$

Chemical Softness $S = \dfrac{1}{\eta}$

Global Electrophilicity $\omega = \dfrac{\mu^2}{\eta}$

Electron donating Power $\omega^- = \dfrac{(3\varepsilon_{HOMO} + \varepsilon_{LUMO})^2}{16\eta}$

Electron accepting Power $\omega^+ = \dfrac{(\varepsilon_{HOMO} + 3\varepsilon_{LUMO})^2}{16\eta}$

Net Electrophilicity $\omega^± = \omega^- + \omega^+$

(4)

The electrophilicity ω scale between 0.8 and 1.5 eV [59, 60] has been used to classify the organic molecules as strong, moderate and marginal electrophiles and HPA falls in the moderate category. The hardness value of 5.322 is indicative of HPA's low chemical reactivity with a potential net electrophilicity value of 5.180.

5. Conclusions

The present study establishes the HPA crystal structure and its preferred supramolecular assemblies, controlled by strong N–H…O and weak C–H…N/O interactions, along with stacking interactions of aromatic π-π type. The dissimilarities of supramolecular constructs observed are ascribed to O–H…N and O–H…O hydrogen bond frameworks. The presence of non-covalent interactions/contacts is the causative factor for producing zig-zag type non-planar sheet and 2D supramolecular layer architecture. The Hirshfeld surface analyses in terms of 2D fingerprint plots and interaction energy calculations corroborate the crystallographic findings. HPA shows exceedingly good SHG activity 1.23 times

Table 7. ^{1}HNMR and^{13}CNMR spectral data of HPA.

Atom/Number	Calculated(δ)	Experimental(δ)
H15	8.461	8.13 (s, 1H)
H16	7.974	8.04 (s, 1H)
H17	5.481	7.18 (s, 2H)
H18	5.071	
H19	3.874	3.96–4.12 (m, 2H)
H20	4.438	
H21	4.158	3.96–4.12 (m, 1H)
H22	1.387	1.06 (d, 3H)
H23	1.383	
H24	1.233	
H25	1.156	5.03 (d, 1H)
C2	159.748	152.3
C4	156.752	149.7
C5	125.367	118.5
C6	160.837	155.9
C8	150.114	141.5
C11	53.589	50.1
C12	73.980	64.6
C13	23.409	20.8

Table 8. Observed (λ_{exp}), computed λ_{max} (λ_{cal}) and excitation energies (E) of HPA.

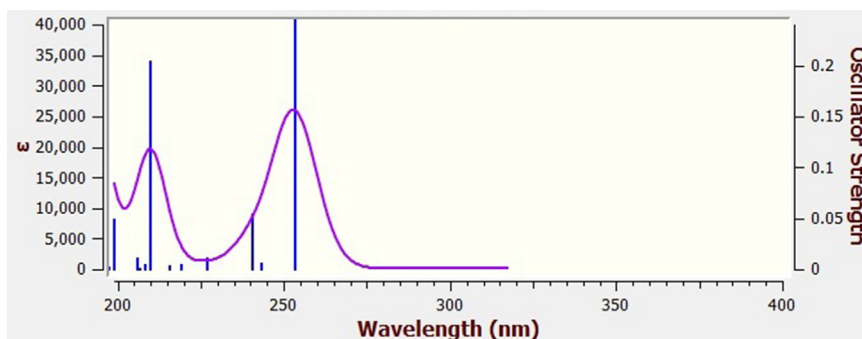| $\lambda_{Exp.}$ (nm)	Excitation No.	$\lambda_{Cal.}$ (nm)	E (eV)	F osc. strength	Assignment
262.00	1	253.25	4.8958	0.2797	π - π*
	7	210.04	5.9029	0.2030	π - π*
206.50	9	206.68	5.999	0.0006	π - π*

Figure 15. Theoretically simulated HPA's UV spectrum.
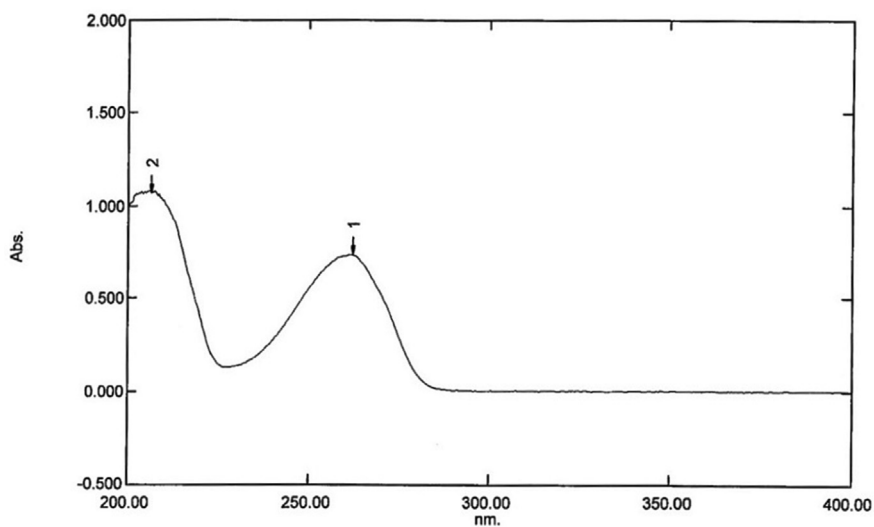
Figure 16. HPA's Experimentally observed UV spectrum.
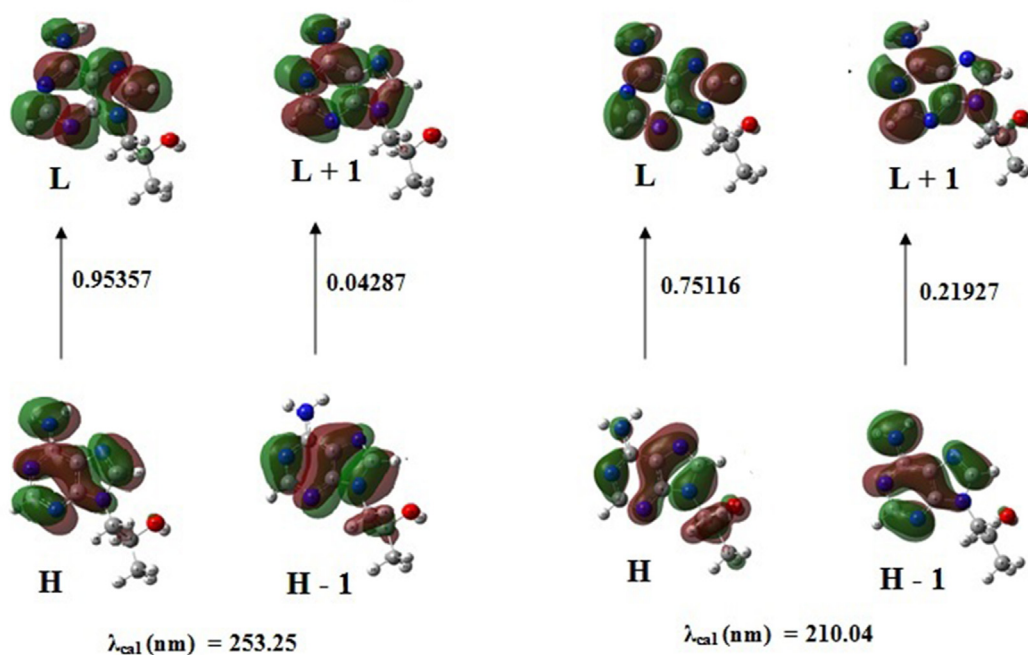
Figure 17. Particle – hole mapping of excited MOs.
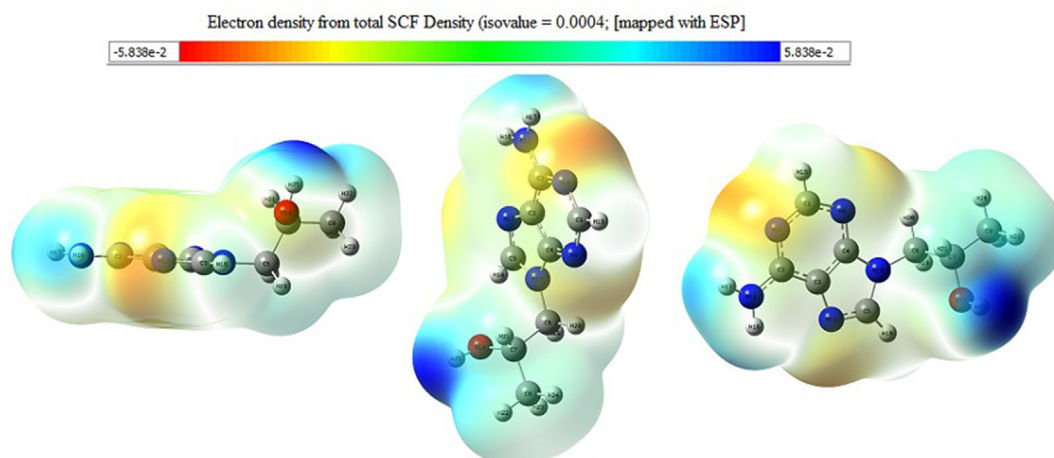
Electron density from total SCF Density (isovalue = 0.0004; [mapped with ESP]

-5.838e-2   5.838e-2

Figure 18. Molecular electrostatic potential map of HPA

LUMO +ve   +   LUMO -ve   LUMO -0.805 eV

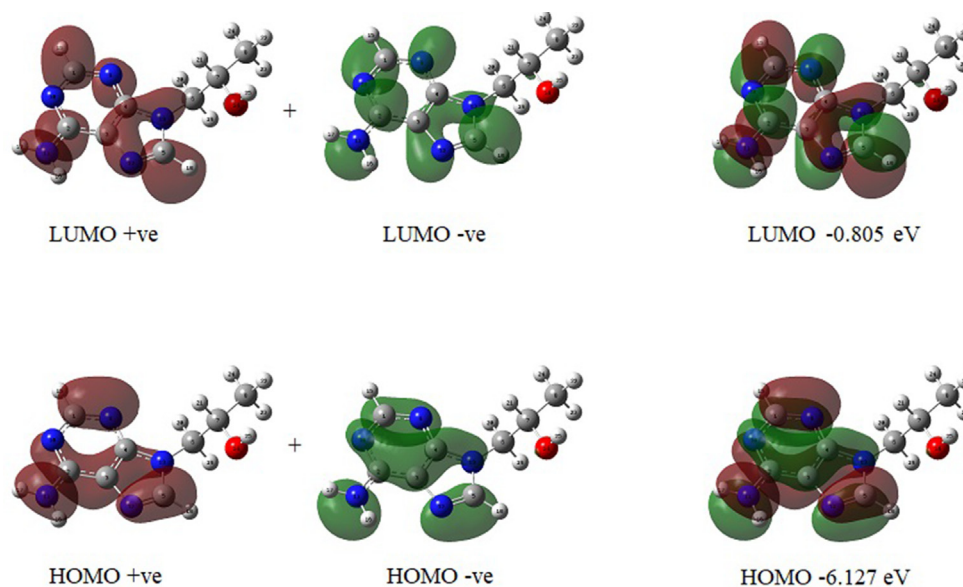HOMO +ve   +   HOMO -ve   HOMO -6.127 eV

Figure 19. HOMO – LUMO structure of HPA.

Table 9. Global chemical reactivity descriptors evaluated at B3LYP/6-311++g (d, p).

S.No	Parameter	Values (eV)
1	ε_{HOMO}	-6.127
2	ε_{LUMO}	-0.805
3	ε_{HLEG}	5.322
4	μ	-3.466
5	η	5.322
6	ω	1.129
7	S	0.188
8	ω^-	4.323
9	ω^+	0.857
10	$\omega^{\pm}$	5.180

higher than that of urea used as the reference sample indicating that further studies could be carried out to explore its use as a potential organic NLO material in the field of optoelectronics. Comparative studies between experimental and theoretical evaluation at B3LYP/6-311++g (d, p) of structural parameters, electronic and resonance magnetic spectra of the title compound have been carried out.

he experimental parameters coincide agreeably with the corresponding quantum chemically calculated values with positive or negative deviations, the cause being the neglect of intermolecular interactions in calculations. The UV-visible spectral analysis in terms of NTOs replaces the canonical MOs with particle-hole intuitions. The electronic structure of the HPA reveals that more electron rich centres N1, N7 and N9are susceptible to protonation, while electron deficient H17, H18 and H25 sites are more prone to nucleophilic attacks. Also the HLEG estimate of 5.322 eV accounts for the stability of the title compound. With all these

characteristic features analysed, the biological activities can be further explored.

Declarations

Author contribution statement

Sharmila Tagore S.: Performed the experiments; Wrote the paper.

Swaminathan J.: Performed the experiments.

Manikandan D., Sabarinathan N.: Contributed reagents, materials, analysis tools or data.

Gomathi S., Ramalingam M.: Analyzed and interpreted the data.

Sethuraman V.: Conceived and designed the experiments; Wrote the paper.

Funding statement

Data availability statement

Data associated with this study has been deposited at www.ccdc.ca m.ac.uk/conts/retrieving.html under the accession number CCDC 1421496.

Declaration of interests statement

The authors declare no conflict of interest.

Additional information

Supplementary content related to this article has been published online at https://doi.org/10.1016/j.heliyon.2021.e06593.

References

[1] M. Bayes, X. Rabasseda, J.R. Prous, Gateways to clinical trials, Methods Find. Exp. Clin. Pharmacol. 25 (2003) 53–76.

[2] L. Jeffery, J.H. Kim, D.F. Wiemer, Synthesis of acyclic nucleoside and nucleotide analogues from amino acids: A convenient approach to a PMEA-PMPA hybrid, Tetrahedron 56 (2000) 5077–5083.

[3] M.J. Keating, Fludarabine phosphate in the treatment of chronic lymphocytic leukemia, Semin. Oncol. 17 (1990) 49–62.

[4] J.A. Montgomery, A.T. Shortnacy-Fowler, S.D. Clayton, J.M. Riordan, J.A. Secrist, Synthesis and biological activity of 2'-fluoro-2-halo derivatives of 9-.beta.-D-arabinofuranosyladenine, J. Med. Chem. 35 (1992) 397–401.

[5] J.A. Secrist, K.N. Tiwari, A.T. Shortnacy-Fowler, L. Messini, J.M. Riordan, J.A. Montgomery, S.C. Meyers, S.E. Ealick, Synthesis and biological activity of certain 4'-Thio-d-arabinofuranosylpurine nucleosides, J. Med. Chem. 41 (1998) 3865–3871.

[6] J.A. Secrist, A. Shortnacy-Fowler, J.A. Montgomery, Synthesis and biological evaluations of certain 2-halo-2'-substituted derivatives of 9-β-d-arabinofuranosyladenine, J. Med. Chem. 31 (1988) 405–410.

[7] E. De Clercq, Strategies in the design of antiviral drugs, Nat. Rev. Drug Discov. 1 (2002) 13–25.

[8] Qun dang, Brain S. Brown, Yan Liu, Robert M. Rydzewski, Edward D. Robinson, Paul D. Van Poelje, M. Rami Reddy, Mark D. Erion, Fructose-1,6-bisphosphatase Inhibitors. 1. purine phosphonic acids as novel AMP mimics, J. Med. Chem. 52 (2009) 2880–2890.

[9] C. Grignet-Debrus, C.M. Calberg-Bacq, Potential of Varicella zoster virus thymidine kinase as a suicide gene in breast cancer cells, Gene Ther. 4 (1997) 560–569.

[10] X.W. Tong, I. Agoulnik, K. Blankenburg, C.F. Contant, A. Hasenburg, L.B. Runnebaum, E. Stickeler, A.L. Kaplan, S.L. Woo, D.G. Kieback, Human epithelial ovarian cancer xenotransplants into nude mice can be cured by adenovirus mediated thymidine kinase gene therapy, Anticancer Res. 17 (1997) 811–813.

[11] G.D. Diana, D. Pevear, D.C. Young, Chapter 14. antiviral agents, Annu. Rep. Med. Chem. 24 (1989) 129–137.

[12] E. De Clereq, Holy, Antiviral activity of aliphatic nucleoside analogs: structure-function relationship, J. Med. Chem. 22 (5) (1979) 510–513.

[13] H.J. Schaeffer, R.N. Johnson, M.A. Schwartz, C.F. Schwender, Enzyme inhibitors. 25. Equation to calculate the unknown Ki from two known values of Ki in an R,S, and RS series. Stereoselectivity of inhibition of adenosine deaminase by (R)-, (S)-,

[14] and (RS)-9-(1-hydroxy-2-alkyl and -aralkyl)adenines, J. Med. Chem. 15 (5) (1972) 456–458.

[14] P. Pospisíl, B.D. Pilger, P. Schelling, C. Wurth, L. Scapozza, G. Folkers, M. Pongracič, M. Mintas, S. Raic-Malic, Synthesis, kinetics, and molecular docking of novel 9-(2-Hydroxypropyl)purine nucleoside analogs as ligands of herpesviral thymidine kinases, Helv. Chim.Acta 85 (2002) 3237–3250.

[15] H.J. Schaeffer, R. Vince, Enzyme inhibitors. XVIII. studies on the stereoselectivity of inhibition of adenosine deaminase by DL-, D-, and L-9-(2-Hydroxypropyl)adenine, J. Med. Chem. 10 (4) (1967) 689–691.

[16] H.J. Schaeffer, R.N. Johnson, M.A. Schwartz, C.E. Schwender, Enzyme inhibitors. 25. Equation to calculate the unknown Ki from two known values of Ki in an R,S, and RS series. Stereoselectivity of inhibition of adenosine deaminase by (R)-, (S)-, and (RS)-9-(1-hydroxy-2-alkyl and -aralkyl)adenines, J. Med. Chem. 15 (1972) 456–459.

[17] H.J. Schaeffer, C.F. Schwender, Enzyme inhibitors. 26. Bridging hydrophobic and hydrophilic regions on adenosine deaminase with some 9-(2-hydroxy-3-alkyl) adenines, J. Med. Chem. 17 (1) (1974) 6–8.

[18] E. De Clercq, J. Descamps, P. De Somer, A. Holy, (S)-9-(2,3-Dihydroxypropyl) adenine: an aliphatic nucleoside analog with broad-spectrum antiviral activity, Science 200 (1978) 563–567.

[19] H.J. Schaeffer, L. Beauchamp, P. de Miranda, G.B. Elion, D.J. Bauer, P. Collins, 9-(2-Hydroxyethoxymethyl)guanine activity against viruses of the herpes group, Nature 272 (1978) 583–585.

[20] G.B. Elion, P.A. Furman, J.A. Fyfe, P. de Miranda, L. Beauchamp, H.J. Schaeffer, The selectivity of action of an antiherpetic agent, 9-(2-hydroxyethoxymethyl) guanine, Proc. Natl. Acad. Sci. Unit. States Am. 74 (1977) 5716–5720.

[21] E. De Clercq, Antiviral activity of aliphatic nucleoside analogs: structure-function relationship, J. Med. Chem. 22 (1979) 510–513.

[22] a) C. Tsai, K E Follis, A. Sabo, T.W. Beck, R.F. Grant, N. Bischofbcrger, R.E. Benveniste, R. Black, Prevention of SIV infection in macaques by (R)-9-(2-Phosphonylmethoxypropyl)adenine, Science 270 (1995) 1197, and references cited therein;
b) L. Naesens, J. Balzarini, E. DeClercq, Antiviral therapy for human immunodeficiency virus infections, Rev. Med. Virol. 4 (1995) 147;
c) C.U. Kim, B.Y. Luh, P.F. Misco, J J Bronson, M.J.M. Hitchcock, I. Ghazzouli, J.C. Martin, Design and synthesis and propranolol analogs as serotonergic agents, J. Med. Chem. 33 (1990) 1207;
d) J.J. Bronson, C.U. Kim, I. Ghazzouli, M.J.M. Hitchcock, E. Kern, J.C. Martin, in: J.C. Martin (Ed.), Nucleosides and Antiviral Agents, American Chemical Society, Washington, DC, 1989, pp. 72–87.

[23] J. Balzarini, S. Aquaro, C.F. Pemo, M. Witvrouw, A. Holy, E. De Clercq, Activity of the (R)-Enantiomers of 9-(2-Phosphonylmethoxypropyl)-Adenine and 9-(2-Phosphonylmethoxypropyl)-2,6-diaminopurine against human immunodeficiency virus in different human cell systems, Biochem. Biophys. Res. Commun. 219 (1996) 337–341.

[24] M. Lisa Schultze, H. Harlan, J.P. Chapman, Dubree Nathan, J. Robert J. Jones, M. Kenneth T. Kent, Thomas Lee, S. Michael, J. Louie, J. Michael, J. Postich, Ernest Prisbe, John C. Rohloff, H.Yu. Richard, Practical synthesis of the anti-HIV drug, PMPA, Tetrahedron Lett. 39 (1998) 1853–1856.

[25] M.D. Erion, K. Takabayshi, H.B. Smith, J. Kessi, S. Wagner, S. Honig, S.L. Shames, S.E. Ealick, Purine nucleoside phosphorylase. 1. structure−function studies, Biochem 36 (1997) 11725–11734.

[26] E.J. Blanzk, F.A. French, J.R. DoAmaral, D.A. French, Carcinostatic activity of thiosemicarbazones of formyl heteroaromatic compounds. VII. 2-Formylpyridine derivatives bearing additional ring substituents, J. Med. Chem. 13 (1970) 1124–1130.

[27] J. Vogt, R. Perozzo, A. Pautsch, A. Prota, P. Schelling, B. Pilger, G. Folkers, L. Scapozza, G.E. Schulz, Nucleoside binding site of Herpes simplex type 1 thymidine kinase analyzed by X-ray crystallography, Proteins 41 (2000) 545–553.

[28] Bruker, SMART APEX2, SAINT ABD SADABS, Bruker AXS Inc., Madison,Wisconsin, USA, 2008.

[29] G.M. Sheldrick, A short history of SHELX, Acta Crystallogr. A64 (2008) 112–122.

[30] A.D. Becke, Densityfunctional thermochemistry. III. The role of exact exchange, J. Chem. Phys. 98 (1993) 5648–5652.

[31] M.J. Frisch, et al., Gaussian 03, Revision E.01, Gaussian Inc., Pittsburgh, PA, 2004.

[32] M.J. Frisch, et al., Gaussian 09, Revision B.01, Gaussian Inc., Pittsburgh, PA, 2010.

[33] F. Ortmann, F. Bechstedt, W.G. Schmidt, Semiempirical van der Waals correction to the density functional description of solids and molecular structures, Phys. Rev. B 73 (2006) 205101.

[34] T. Steiner, C–H⋯O hydrogen bonding in crystals, Crystallogr. Rev. 9 (2–3) (2003) 177–228.

[35] M.J. Turner, J.J. Mckinnon, S.K. Wolff, D.J. Grimwood, P.R. Spackman, D. Jayatilaka, M.A. Spackman, CrystalExplorer 17.5, The University of Western Australia, 2017.

[36] P. Venkatesan, S. Thamotharan, A. Ilangovan, H. Liang, T. Sundius, Crystal structure, Hirshfeld surfaces and DFT computation of NLO active (2E)-2-(ethoxycarbonyl)-3-[(1-methoxy-1-oxo-3-phenylpropan-2-yl)amino] prop-2-enoic acid, Spectrochim. Acta 153 (2016) 625–636.

[37] M.A. Spackman, D. Jayatilaka, Hirshfeld surface analysis, CrystEngComm 11 (2009) 19–32.

[38] S.S. Batsanov, Van der Waals Radii of Elements, Inorg. Mater. 37 (9) (2001) 871–885.

[39] M.J. Turner, S. Grabowsky, D. Jayatilaka, M.D. Spackman, Accurate and efficient model energies for exploring intermolecular interactions in molecular crystals, J. Phys. Chem. Lett. 5 (2014) 4249–4255.

[40] S.K. Kurtz, T.T. Perry, A powder technique for the evaluation of nonlinear optical materials, J. Appl. Phys. 39 (1968) 3798–3813.

[41] P. Pospisil, B.D. Pilger, S. Marveggio, P. Schelling, C. Wurth, L. Scapozza, G. Folkers, M. Pongracic, M. Mintasand, S.R. Malic, Synthesis, kinetics, and molecular docking of novel 9-(2-Hydroxyprpoyl)purine nucleoside analogs as ligands of herpesviral thymidine kinases, Helv. Chim. Acta 85 (2002) 3237–3250.

[42] R.L. Martin, Natural transition orbitals, J. Chem. Phys. 118 (2003) 4775–4777.

[43] J.H. Schachtschneider, Technical Report (Shell Development Company), Emery Ville, ,CA, USA, 1964, 65.

[44] C.F. Matta, R.J. Gillespie, Understanding and interpreting molecular electron densitydistributions, J. Chem. Educ. 79 (9) (2002) 1141–1152.

[45] I. Fleming, Frontier Orbitals and Organic Chemical Reactions, John Wiley and Sons, Berlin, 1976.

[46] J.S. Murray, K. Sen, Molecular Electrostatic Potentials, Concepts and Applications, Elsevier, Amsterdam, 1996.

[47] N. Okulik, A.H. Jubert, Theoretical analysis of the reactive sites of non–steroidal anti–inflammatory drugs, J. Mol. Des. (2005) 4–17.

[48] C.J. Cramer, Essentials Computational Chemistry, Wiley, Hoboken, NJ, 2004.

[49] R. Stowasser, R. Hoffmann, What do the Kohn−Sham orbitals and eigenvalues mean? J. Am. Chem. Soc. 121 (1999) 3414–3420.

[50] G. Zhang, Charles B. Musgrave, Comparison of DFT methods for molecular orbital eigenvalue calculations, J. Phys. Chem. 111 (2007) 1554–1561.

[51] C.G. Zhan, J.A. Nichols, D.A. Dixon, Ionization potential, electron affinity, electronegativity, hardness, and electron excitation energy: molecular properties from density functional theory orbital energies, J. Phys. Chem. 107 (2003) 4184–4195.

[52] S. Gunasekaran, R. ArunBalaji, S. Kumaresan, G. Anand, S. Srinivasan, Experimental and theoretical investigations of spectroscopic properties of N-acetyl-5-methoxytryptamine, Can. J. Anal. Sci. Spectrosc. 53 (2008) 149.

[53] D.F.V. Lewis, C. Ioannides, D.V. Parke, Interaction of a series of nitriles with the alcohol-inducible isoform of P450: computer analysis of structure-activity relationships, Xenobh 24 (5) (1994) 401–408.

[54] L. Padmaja, C. Ravikumar, D. Sajan, I.H. Joe, V.S. Jayakumar, G.R. Pettict, O.F. Nielson, Density functional study on the structural conformations and intramolecular charge transfer from the vibrational spectra of the anticancer drug combretastatin-A2, J. Raman Spectrosc. 40 (2009) 419–428.

[55] C. Ravikumar, I.H. Joe, V.S. Jayakumar, Charge transfer interactions and nonlinear optical properties of push–pull chromophore benzaldehyde phenylhydrazone: A vibrational approach, Chem. Phys. Lett. 460 (2008) 552–558.

[56] A. Pirnau, O. Chis, N. Oniga, L. Leopold, M. Szabo, O. Baias, O. Cozar, Vibrational and DFT study of 5-(3-pyridyl-methylidene)-thiazolidine-2-thione-4-one, Vib. Spectrosc. 48 (2008) 289–296.

[57] S. Liu, Dynamic behavior of chemical reactivity indices in density functional theory: A Bohn-Oppenheimer quantum molecular dynamics study, J. Chem. Sci. 117 (5) (2005) 477–483.

[58] N. Flores-Holguín, J. Frau, D. Glossman-Mitnik, Chemical reactivity and bioactivity properties of the Phallotoxin family of fungal peptides based on Conceptual Peptidology and DFT study, Heliyon 5 (8) (2019), 1-6.

[59] P. Patricia, Theoretical Aspects of Chemical Reactivity 19, 2007, pp. 139–201. Chapter 9.

[60] H. Jangra, Q. Chen, E. Fuks, I. Zenz, P. Mayer, A.R. Ofial, H. Zipse, H. May, Nucleophilicity and electrophilicity parameters for predicting absolute rate constants of highly asynchronous 1,3-Dipolar cycloadditions of aryldiazomethanes, J. Am. Chem. Soc. 140 (48) (2018) 16758–16772.